

pubs.acs.org/JPCC Article

Irreversibility in Anion Exchange Between Cesium Lead Bromide and Iodide Nanocrystals Imaged by Single-Particle Fluorescence

Dong Wang, Dongyan Zhang, and Bryce Sadtler*



Cite This: https://dx.doi.org/10.1021/acs.jpcc.0c08323



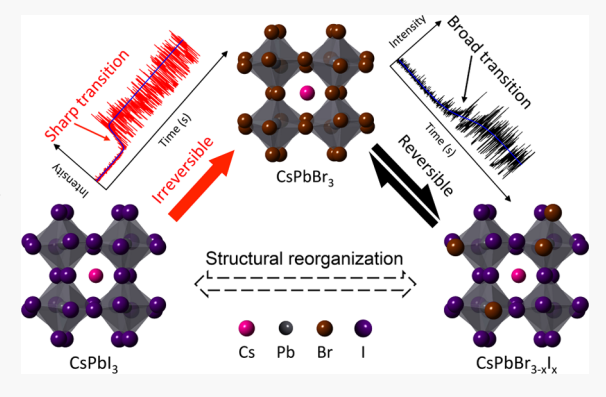
ACCESS

III Metrics & More

Article Recommendations

Supporting Information

ABSTRACT: Anion exchange is a powerful method to tune the emission wavelength of perovskite CsPbX₃ (X = Cl, Br, or I) nanocrystals across the visible spectrum. CsPbX₃ nanocrystals can possess a number of crystal structures that depend on both their composition and size. Understanding the role these structural variations play during anion exchange is important for their future application in optoelectronic devices. In this work, we used fluorescence microscopy to monitor reaction trajectories of individual nanocrystals as they undergo anion exchange between CsPbBr₃ and CsPbI₃. By varying the concentration of substitutional ion used to induce anion exchange, we quantify differences in reaction times for exchange in opposite directions. CsPbI₃ nanocrystals undergo more abrupt shifts in their emission characteristics as they transform to CsPbBr₃, while CsPbBr₃ nanocrystals exhibit a smoother transition during



their transformation to CsPbI₃. Simulations of anion exchange using Monte Carlo trajectories are consistent with a larger degree of structural reorganization when CsPbI₃ nanocrystals undergo anion exchange. Together, these results reveal that there are structural differences between CsPbI₃ nanocrystals synthesized by the hot-injection method and those produced by anion exchange. The narrower distribution of reaction times when CsPbI₃ nanocrystals transform to CsPbBr₃ may produce better compositional homogeneity when this reaction is scaled-up to incorporate these materials into optoelectronic devices.

■ INTRODUCTION

Lead halide perovskite semiconductors with the formula APbX₃ (where $A = CH_3NH_3^+$ or Cs^+ and $X = Cl^-$, Br^- , or I^-) are widely studied for applications in optoelectronic devices, including solar cells and light-emitting diodes (LEDs).¹⁻⁷ The high photoluminescence (PL) quantum yields, tunable bandgap, and facile synthesis of colloidal CsPbX3 nanocrystals (NCs) make them especially attractive for light-emission applications.^{6–14} Starting with one initial composition prepared by the hotinjection method (e.g., CsPbBr₃), the emission wavelength of CsPbX₃ NCs can be tuned across the entire visible spectrum via anion exchange to CsPbBr_{3-x}I_x or CsPbBr_{3-x}Cl_x. ^{10-12,15-20} To maximize color purity for light-emission applications, it is critical to have high uniformity in structure and composition among the population of NCs. Early reports on anion exchange indicated that mixed-halide CsPbBr_{3-x}Cl_x and CsPbBr_{3-x}I_x NCs form homogeneous solid solutions at all phase fractions (i.e., all values of x). $^{15-17}$ However, recent work has shown that mixed-halide lead perovskite crystals can possess structural and compositional heterogeneity, 20'-24 which will be deleterious for their applications in optoelectronic devices.

The solid-state miscibility between two crystalline compounds reflects the degree of similarity in their structure. CsPbCl₃ and CsPbBr₃ are miscible at all phase fractions at room temperature, while CsPbCl₃ and CsPbI₃ are immiscible due to the large difference in anion size and electronegativity. ^{25,26}

CsPbBr₃ and CsPbI₃ possess intermediate miscibility. The structures of CsPbBr₃, CsPbI₃, and mixed-halide CsPbBr_{3-x}I_x NCs have been reported to possess either the perovskite cubic α phase, $^{15-17}$ the perovskite orthorhombic γ phase, 12,22,27 or the nonperovskite orthorhombic δ phase (i.e., yellow phase)²⁸ depending on the method used to prepare the NCs (e.g., hotinjection synthesis with mixed-halide precursors vs postsynthetic anion exchange), the method used to determine the structure (e.g., conventional powder X-ray diffraction (XRD) vs synchrotron-based X-ray scattering), and the amount of time between sample preparation and structure measurement. Furthermore, recent studies on CsPbX3 NCs synthesized by the hot-injection method have shown that the presence of sizedependent surface strain²⁹ and coherent twin boundaries²² can lead to variations in the tilting of corner-sharing PbX₆ octahedra that make up the perovskite structure. While these investigations have not yet been extended to CsPbX₃ NCs prepared by anion exchange, we anticipate that subtle differences in the structure of

Received: September 12, 2020 Revised: November 13, 2020



the parent nanocrystals may lead to different degrees of structural reorganization as CsPbX₃ nanocrystals undergo anion exchange. Thus, it is critical to have an *in situ* method to probe how differences in the structure of CsPbX₃ nanocrystals affect their chemical reactivity.

Single-particle optical measurements remove ensemble averaging to reveal differences in chemical and physical behavior among nanocrystals prepared within the same synthetic batch. 13,14,30-43 We and others have used single-particle fluorescence microscopy to monitor chemical transformations in semiconductor NCs including cation exchange, anion exchange, and ion intercalation based on changes in the emission intensity and wavelength of individual NCs as they transform. 39-43 These measurements quantify heterogeneity in the reaction times for a population of NCs undergoing the same transformation. In every system studied so far, the switching times, which characterize the rate at which the PL intensity changes for individual NCs, are much shorter than the time it takes for the ensemble of NCs to transform. However, each NC exhibits a different characteristic waiting time before it begins to transform, which leads to a gradual change in PL intensity for the ensemble of NCs. The difference in structure between the initial and final crystals controls the variance in reactivity among the population of NCs. Immiscible crystal pairs (e.g., CdSe/Ag₂Se and PbBr₂/CH₃NH₃PbBr₃) that require a substantial reorganization of both cations and anions exhibit shorter waiting and switching times compared to highly miscible systems (e.g., CsPbCl₃/CsPbBr₃) in which a phase transformation does not occur.^{39–42} Furthermore, the switching times for miscible systems show a stronger dependence on the concentration of the substitutional ion.

In this work, we used single-particle fluorescence microscopy to image anion exchange in CsPbBr₃ and CsPbI₃ nanocrystals. We observed asymmetric behavior at both the ensemble and single-particle levels when the interconversion between CsPbBr₃ and CsPbI3 proceeded in opposite directions. We develop a simple kinetic model that captures this asymmetric behavior based on the degree of reorganization of the crystal lattice during the transformation. CsPbI₃ NCs undergo a larger change in structure as they transform to CsPbBr₃ compared to when CsPbBr₃ NCs transform to CsPbI₃. The more abrupt change leads to a narrower distribution of reaction times when assynthesized CsPbI₃ NCs undergo anion exchange to CsPbBr₃. Our study reveals that anion exchange between CsPbBr3 and CsPbI₃ is not completely reversible. Structural differences between CsPbX₃ NCs directly synthesized by the hot-injection method and those prepared by anion exchange lead to differences in their chemical reactivity.

EXPERIMENTAL SECTION

Materials. The following chemicals were used as received: cesium carbonate (Cs_2CO_3 , 99%, Millipore Sigma Inc.), lead(II) iodide (PbI₂, 99%, Millipore Sigma Inc.), lead(II) bromide (PbBr₂, >98%, Alfa Aesar), oleic acid (90%, Millipore Sigma Inc.), oleylamine (70%, Millipore Sigma Inc.), *tert*-butanol (anhydrous, ≥99.5%, Millipore Sigma Inc.), hexane (anhydrous, 95%, Millipore Sigma Inc.), 1-octadecene (ODE, tech. 90%, Alfa Aesar), toluene (anhydrous, 99.8%, Millipore Sigma Inc.), tetrabutylammonium bromide (TBAB, ≥98%, Millipore Sigma Inc.), and tetrabutylammonium iodide (TBAI, ≥98%, Millipore Sigma Inc.).

Synthesis of Cesium Lead Halide Perovskite Nanocrystals. The hot-injection method reported by Kovalenko and

co-workers was adapted to synthesize colloidal cesium lead iodide (CsPbI₃) and cesium lead bromide (CsPbBr₃) nanocrystals (NCs).8 Instead of drying the oleic acid and oleylamine separately, we mixed these surfactants with the other precursors (i.e., Cs₂CO₃ or PbX₂) and dried them together. In a typical synthesis, 102 mg of Cs₂CO₃, 0.32 mL of oleic acid, and 5 mL of ODE were added to a 50 mL, round-bottom flask (labeled as Flask I). For the synthesis of CsPbI₃, 87 mg of PbI₂, 0.7 mL of oleylamine, 0.7 mL of oleic acid, and 5 mL of ODE were added into another 50 mL, round-bottom flask (labeled as Flask II). For the synthesis of CsPbBr3, 69 mg of PbBr2, 1 mL of oleylamine, 1 mL of oleic acid, and 5 mL of ODE were added to Flask II. Both flasks were connected to a Schlenk line. Flask I was heated at 120 °C under vacuum for 1 h and then heated at 150 °C under an argon atmosphere for another hour. Flask II was heated at 100 °C under vacuum for 1 h. Then, Flask II was switched to an argon environment, and the temperature was elevated to 170 °C. Next, 0.4 mL of the solution from Flask I was removed using a syringe and quickly injected into Flask II. After 60 s, Flask II was quenched in an ice bath. After cooling, the mixture in Flask II was centrifuged at 8000 rpm for 5 min. The precipitate was collected, dispersed in 10 mL of anhydrous hexane, and stored in a nitrogen-filled glovebox for future use.

Photoluminescence (PL) Spectroscopy. PL spectra were measured using a Cary Eclipse fluorescence spectrophotometer. The scan rate was set to medium, and the step size was 1 nm. The slit widths for excitation and emission were adjusted between 2.5 and 10 nm to obtain spectra with maximum intensities of around 500 counts. The excitation wavelength was 400 nm.

Anion exchange reactions between CsPbBr₂ and CsPbI₂ NCs in colloidal solution were monitored at the ensemble level by PL spectroscopy. TBAI was used to transform CsPbBr₃ NCs into CsPbI₃, and TBAB was used to transform CsPbI₃ NCs into CsPbBr₃. To prepare each sample, the stock solution of CsPbBr₃ or CsPbI₃ NCs was first diluted by a factor of 100 by adding 50 μL of the stock solution to 5 mL of hexane. Then, 1.5 mL of the diluted CsPbX3 solution and 1 mL of hexane were added to a quartz cuvette. First, a PL spectrum of the initial CsPbX3 NCs was measured. Then, aliquots of either the TBAB or TBAI solution (0.3 mg/mL in tert-butanol) were added sequentially to the cuvette. The volume of TBAB/TBAI for each addition was 60 and 80 μ L, respectively. After each addition, the cuvette was vigorously shaken for 30 s before measuring the PL spectrum. Anion exchange was considered complete when further addition of the TBAB/TBAI solution led to shifts in the PL spectra of less than 2 nm.

Single-Particle Fluorescence Imaging. Fluorescence microscopy was performed using a Nikon N-STORM microscopy system consisting of a Nikon TiE motorized inverted optical microscope and a Nikon CFI-6-APO TIRF 100× oil-immersion objective lens with a numerical aperture of 1.49 and a working distance of 210 μ m. A white-light LED (Xcite 120 LED) was used as the excitation source. Dilute solutions of the CsPbX₃ NCs were spin-coated onto microscope coverslips and assembled into flow cells. See the Supporting Information (SI) and our previous work for additional details on sample preparation. 41,42 Diluting the stock solution of CsPbX₃ NCs by a factor of 500 before spin coating provided a sufficient number of NCs in the microscope field-of-view to gather statistics of the reaction trajectories while minimizing the number of clusters of particles. No further preparation was needed for the majority of NCs to remain fixed to the substrate while imaging anion exchange. To watch the transformation of

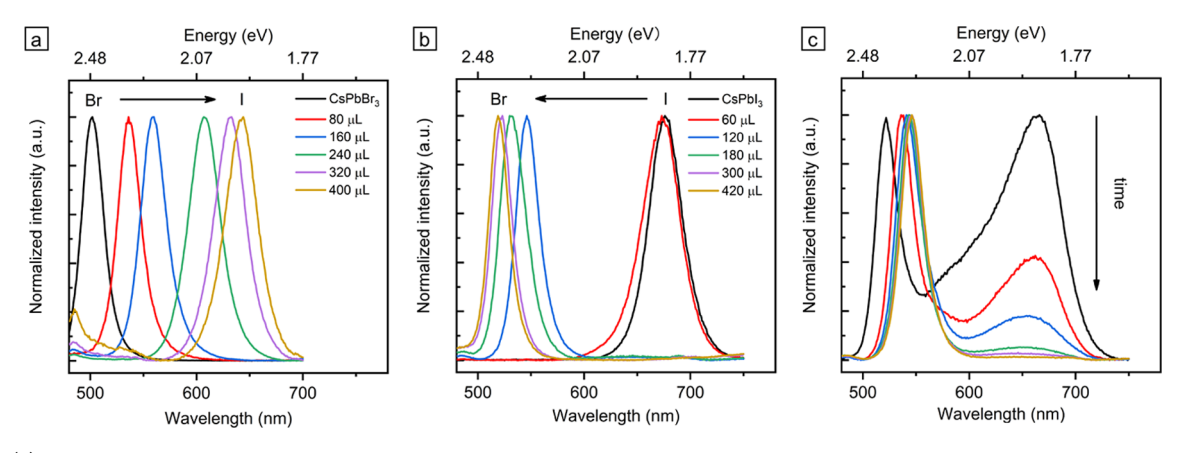


Figure 1. (a) PL spectra showing the transformation of CsPbBr₃ NCs to CsPbI₃ through the addition of increasing amounts of a TBAI solution in *tert*-butanol with a concentration of 0.3 mg/mL (0.81 mmol/L). (b) PL spectra showing the transformation of CsPbI₃ NCs to CsPbBr₃ through the addition of increasing amounts of a TBAB solution in *tert*-butanol with a concentration of 0.3 mg/mL (0.93 mmol/L). (c) Temporal evolution of the PL spectra over an approximately 8 min period after the addition of two aliquots of the TBAB solution (120 μ L total) to a solution of CsPbI₃ NCs. Each acquisition took approximately 30 s, and there were 1 min intervals between spectra. All PL spectra were normalized to the same maximum intensity, and the excitation wavelength was 400 nm for all spectra.

CsPbI₃ NCs to CsPbBr₃, we first used a red filter set (Chroma #49005-ET-DSRed, excitation window: 530-558 nm, emission window: 590-649 nm) to focus on emission from the initial CsPbI₃ NCs. We then switched to a green filter set (Chroma #49002-ET-EGFP, excitation window: 450-490 nm, emission window: 500-540 nm) to image anion exchange. In this case, the initial field-of-view is dark, and individual NCs become bright as they undergo anion exchange. A solution of ODE and tert-butanol (25:1 volume ratio) was first flowed into the flow cell. Next, a solution of TBAB in ODE and tert-butanol (25:1 volume ratio) was flowed into the cell to trigger anion exchange. The flow rate was fixed at 20 mL/h by a syringe pump. The concentrations of TBAB used were 1, 2, 3, 4, 6, and 10 μ g/mL (i.e., 3.1, 6.2, 9.3, 12.4, 18.6, and 31.0 μ mol/L). Fluorescent videos were recorded at a light intensity of $\sim 29 \,\mu\text{W/cm}^2$ at the focal plane using the green filter set. An Andor iXon 897 electron-multiplying CCD camera (512 \times 512, 16 μ m pixels, >90% quantum efficiency) was used to detect fluorescence signals, and the exposure time was 20 ms.

To watch the transformation of CsPbBr₃ NCs to CsPbI₃, we first used the green filter set to focus on emission from the initial CsPbBr₃ NCs and then switched to the red filter set to watch the turn-on in emission as NCs underwent anion exchange. Solutions of TBAI in ODE and tert-butanol (25:1 volume ratio) were used to trigger anion exchange. The concentrations of TBAI used were 1, 2, 3, 4, 6, and 10 μ g/mL (i.e., 2.7, 5.4, 8.1, 10.8, 16.2, and 27.0 μ mol/L). Fluorescent videos were recorded at a light intensity of $\sim 18 \,\mu\text{W/cm}^2$ at the focal plane using the red filter set and an exposure time of 20 ms. For the back conversion of CsPbBr_{3-x}I₃ NCs that had already undergone anion exchange, the green filter set was used to watch the conversion back to CsPbI3, and the red filter set was used to watch conversion back to CsPbBr3. For each of these transformations, the initial field-of-view was bright, and the NCs became dark as they underwent anion exchange.

■ RESULTS AND DISCUSSION

Ensemble Fluorescence Spectroscopy. $CsPbX_3$ (X = Br or I) nanocrystals were synthesized using the hot-injection method developed by Kovalenko and co-workers (see the Experimental Section for further details). Different halide sources have previously been used to induce anion exchange in

 $CsPbX_3$ NCs including lead halide salts, alkylammonium halides, and trimethylsilyl halides. $^{10-12,15-20}$ We have found that tetrabutylammonium halides dissolved in a mixture of tertbutanol and a nonpolar solvent (either hexane or 1-octadecene) induce anion exchange while minimizing degradation of the NCs as evidenced by the ensemble and single-particle fluorescence. 42 We first studied the interconversion between CsPbBr3 and CsPbI3 NCs at the ensemble level using photoluminescence (PL) spectroscopy. CsPbBr₃ NCs were transformed to CsPbI₃ by successively adding 80 µL aliquots of a solution of tetrabutylammonium iodide (TBAI, 0.3 mg/mL = 0.81 mmol/L in tert-butanol) to a hexane solution of CsPbBr₃ NCs. The cuvette was shaken after the addition of each aliquot, and it took less than 30 s for the emission maximum to stop shifting after adding the TBAI solution. Therefore, following each addition, we allowed anion exchange to proceed for 30 s before acquiring a PL spectrum. PL spectra of the as-synthesized CsPbBr₃ NCs and resulting mixed-halide CsPbBr_{3-x}I_x NCs are shown in Figure 1a. The emission maxima continuously redshifted from 502 to 643 nm as five aliquots of the TBAI solution were added. The full width at half maximum (FWHM) of the PL spectra was similar for both initial CsPbBr₃ NCs (0.13 eV) and iodide-rich CsPbBr_{3-x}I_x NCs (0.11 eV) following the final aliquot of TBAI (see Table S1). Assuming a linear change in bandgap energy with composition, ¹⁹ the composition of the product NCs after the total addition of 400 μ L of the TBAI solution (0.32 μmol of TBAI) was CsPbBr_{0.3}I_{2.7}. Further addition of TBAI led to a minimal shift (i.e., <2 nm) of the resulting PL spectra.

CsPbI₃ NCs were transformed to CsPbBr₃ by successively adding 60 μ L aliquots of a solution of tetrabutylammonium bromide (TBAB, 0.3 mg/mL = 0.93 mmol/L in *tert*-butanol) to a hexane solution of CsPbI₃ NCs (Figure 1b). After the second aliquot (i.e., 120 μ L total of the TBAB solution), the resulting spectrum of the mixed-halide CsPbBr_{3-x}I_x NCs changed over the course of several minutes. The temporal evolution of the PL spectra after the second aliquot is shown in Figure 1c. The PL spectrum first splits into two peaks, one centered at 522 nm and the other at 666 nm (corresponding to CsPbBr_{2.6}I_{0.4} and CsPbBr_{0.1}I_{2.9}, respectively). Over a period of several minutes, the peak centered at 666 nm decreased in intensity, while the peak originally centered at 522 nm red-shifted in its peak maximum to

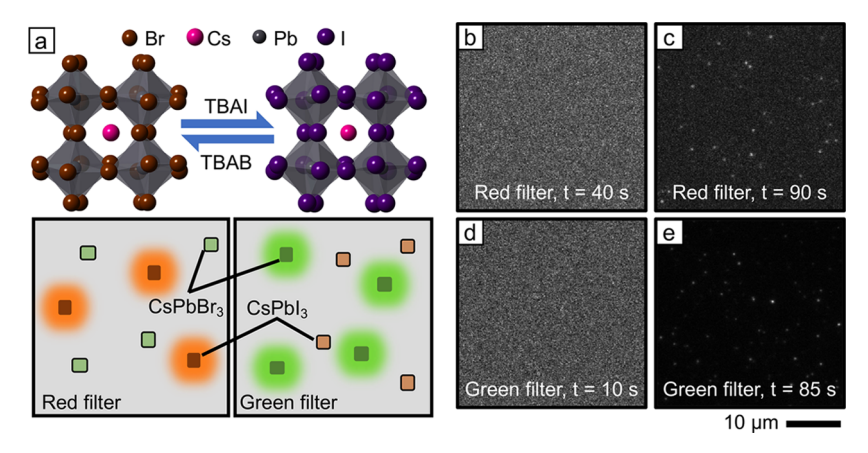


Figure 2. (a) Models of CsPbBr₃ and CsPbI₃ crystals with the perovskite orthorhombic γ phase (top) and illustrations of the microscope field-of-view under different excitation conditions (bottom). Emission from CsPbI₃ NCs is detected using the red filter set, and emission from CsPbBr₃ NCs is detected using the green filter set. (b, c) Fluorescence video frames before and after the transformation of CsPbBr₃ NCs to CsPbI₃ using TBAI. (d, e) Fluorescence video frames before and after the transformation of CsPbBr₃ using TBAB. Only portions of the entire field-of-view are shown in (b-e).

546 nm (corresponding to CsPbBr_{2.2}I_{0.8}). Similar to the transformation of CsPbBr₃ to CsPbI₃, subsequent additions of TBAB required less than 30 seconds for the peak maximum to stop shifting (Figure 1b). The FWHM of the PL spectra was similar for both initial CsPbI₃ NCs (0.11 eV) and bromide-rich CsPbBr_{3-x}I_x NCs (0.11 eV) following the final aliquot of TBAB (see Table S2). Based on its peak maximum at 519 nm, the composition of the product NCs after a total of 420 μ L of the TBAB solution (0.39 μ mol of TBAB) was CsPbBr_{2.6}I_{0.4}. When 420 μ L of the TBAB solution was added all at once rather than in 60 μ L aliquots, the PL spectrum was also observed to first split into two peaks and then merge into a single peak centered at 518 nm after several minutes (Figure S1).

Thus, two populations of nanocrystals, one iodide-rich and one bromide-rich, were readily observable during the ensemble transformation of CsPbI₃ NCs to CsPbBr₃ but not during the transformation of CsPbBr₃ NCs to CsPbI₃ (at the time scale that the steady-state PL spectra were obtained). The continuous redshifting of PL spectra with successive TBAI addition during the transformation of CsPbBr3 NCs to CsPbI3 closely resembles systems in which the initial and final crystals possess high solid solubility, such as anion exchange between CsPbCl₃ and CsPbBr₃ NCs^{15,25,42} or cation exchange between CdTe and HgTe NCs. 44 On the other hand, the abrupt shift in PL peak position during the transformation of CsPbI₃ NCs to CsPbBr₃ with increasing TBAB addition bears similarity to NC transformations in which the initial and final crystals lack miscibility, such as the conversion of CdSe to Ag₂Se NCs via cation exchange. In this reaction, optical spectra can be assigned to linear combinations of purely CdSe and purely Ag₂Se NC spectra with no identifiable intermediates.^{39,45} In the transformation of CsPbI₃ NCs to CsPbBr₃, the two populations of NCs show partial miscibility based on the shifts in peak maxima for the bromide-rich and iodide-rich fractions.

Structural Characterization. Characterization of the CsPbX₃ NCs before and after anion exchange using bright-field transmission electron microscopy (TEM) and X-ray diffraction (XRD) is shown in Figures S2–S5 of the Supporting Information. Due to slow degradation of the CsPbX₃ NCs even when stored in a nitrogen-filled glovebox over the course of several months and laboratory shutdowns amidst the Covid-19 pandemic, these structural characterizations were performed on

different batches of CsPbBr₃ and CsPbI₃ NCs (prepared using the same reaction conditions) than the ones used for ensemble and single-particle fluorescence. Ensemble PL spectra of the different batches of NCs are shown in Figure S6. The PL maxima and FWHM for both CsPbBr₃ samples are nearly identical, and the same is true for both CsPbI3 samples. Table S3 in the Supporting Information matches data shown in each figure with the sample that was used. The as-synthesized CsPbBr₃ and CsPbI₃ NCs have a platelet shape with average edge lengths of 9.4 ± 1.5 nm and 11.3 ± 2.5 nm (average \pm 1st standard deviation), respectively (Figures S2 and S3). Anion exchange was performed by drop casting a solution of either TBAI onto CsPbBr₃ NCs or TBAB onto CsPbI₃ NCs dispersed on a TEM grid. Histograms of the edge lengths before and after anion exchange are provided in Figure S3 and show that the original size and shape of the NCs are preserved after anion exchange. The expected change in lateral dimensions after anion exchange based on the larger lattice volume of CsPbI3 compared to CsPbBr₃ is within the first standard deviation of the size distributions for these batches of NCs. Thus, we do not observe a significant change in the average edge length after anion exchange, similar to previous work.

X-ray diffraction (XRD) patterns of the CsPbX₃ NCs before and after anion exchange are shown in Figure S4. The patterns of all samples matched most closely with simulated patterns for the respective perovskite orthorhombic γ phase of CsPbX₃. For example, the as-synthesized CsPbI₃ NCs possess peaks that are present in the orthorhombic γ phase of CsPbI₃ but absent in the cubic α phase. Additionally, peaks indicative of the nonperovskite δ phase in the initial CsPbI₃ sample are absent. The XRD patterns displayed the expected peak shifts to smaller angles when CsPbBr₃ NCs were converted to CsPbI₃ and to larger angles when CsPbI₃ NCs were converted to CsPbBr₃. However, similar to the ensemble PL spectra described above, the XRD patterns indicate that the NCs still contained a residual amount of the parent anion after exchange, even when an excess of the substitutional anion was used. At the high concentrations of NCs needed to prepare samples for XRD (relative to samples used for ensemble PL and TEM described above), some aggregation and degradation was observed in the samples after anion exchange as evidenced by narrower peaks (indicating larger crystallite size) and the presence of peaks belonging to the

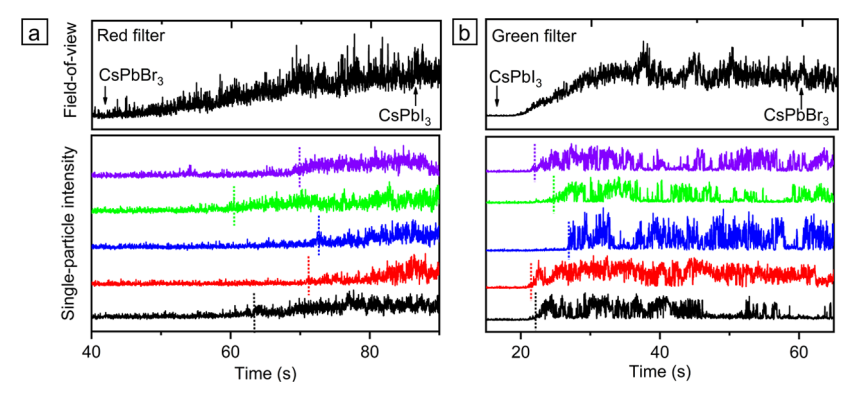


Figure 3. Fluorescence intensity trajectories for CsPbX₃ NCs undergoing anion exchange. (a) Intensity trajectory over the entire field-of-view (top) along with representative trajectories for individual NCs (bottom) during the transformation of CsPbBr₃ NCs to CsPbI₃ using TBAI at a concentration of 1 μ g/mL (2.7 μ mol/L). The single-particle trajectories have been vertically offset for clarity. (b) Intensity trajectory over the entire field-of-view (top) along with representative trajectories for individual NCs (bottom) during the transformation of CsPbI₃ NCs to CsPbBr₃ using TBAB at a concentration of 1 μ g/mL (3.1 μ mol/L). The vertical dashed lines in the individual trajectories mark the waiting time for the NC.

nonperovskite δ phase as an impurity in CsPbI₃ NCs produced by anion exchange (see Figure S5). The potential effects of particle degradation should be minimal in the fluorescence microscopy studies described below. The NCs are fixed to a glass substrate such that aggregation during anion exchange cannot occur. Furthermore, the nonperovskite δ phase of CsPbI₃ is nonfluorescent and therefore will not be detected during fluorescence imaging.

Single-Particle Fluorescence Imaging. Further interpretation of the PL spectra shown in Figure 1 is limited as the observed spectral shifts are averaged over all nanocrystals in the cuvette, which are undergoing different rates of anion exchange. Thus, we used single-particle PL microscopy to understand the origins of the asymmetric behavior observed for anion exchange between CsPbBr₃ and CsPbI₃ NCs. The change in the emission wavelength and intensity for individual NCs provides a signature of their transformation. ^{39–42} We prepared samples for singleparticle imaging by spin-coating dilute solutions of CsPbX₃ NCs onto microscope coverslips. Each sample was then assembled into a home-made flow cell used to introduce the substitutional anion, either TBAI or TBAB dissolved in tert-butanol and 1octadecene (additional details on sample preparation are provided in the Experimental Section and SI). We used two different filter sets to image the transformation between CsPbBr₃ and CsPbI₃ NCs. A red filter set (Chroma #49005-ET-DSRed, excitation window: 530–558 nm, emission window: 590-649 nm) was used to image the conversion of CsPbBr₃ NCs to CsPbI₃. As illustrated in Figure 2a, the red filter blocks emission from the initial CsPbBr₃ NCs but transmits emission from iodide-rich CsPbBr_{3-x} I_x NCs (for $2.7 \ge x \ge 1.7$ assuming a linear relationship between bandgap and halide composition). Consequently, the initial field-of-view is dark for this transformation (Figure 2b). After the TBAI is injected into the flow cell, fluorescent spots begin to appear (Figure 2c and Supporting Information Movie M1). We also transformed CsPbBr₃ NCs to iodide-rich CsPbBr_{3-x} I_x prior to imaging (see the SI for details) and then watched their back conversion to CsPbBr₃ by monitoring the turn off in emission of individual NCs with the same red filter set (Supporting Information Movie M2). Conversely, a green filter set (Chroma #49002-ET-EGFP, excitation window: 450-490 nm, emission window: 500-540 nm) was used to block emission from CsPbI₃ NCs but transmit emission from bromide-rich CsPbBr_{3-x} I_x NCs (for $0 \le x \le 2$ assuming a linear relationship between bandgap and halide

composition). We imaged the conversion of CsPbI₃ NCs to CsPbBr₃ using the green filter set in which the turn-on in emission indicates the transformation of each NC (Figure 2d,e and Supporting Information Movie M3). We also transformed CsPbI₃ NCs to bromide-rich CsPbBr_{3-x}I_x prior to imaging and then watched their back conversion to CsPbI₃ by monitoring the turn off in emission of individual NCs (Supporting Information Movie M4). We note that ensemble PL and XRD indicate the exchange reaction is not complete even when an excess of substitutional anions is used, similar to a previous report. For simplicity, we refer to NCs after anion exchange as CsPbBr₃ or CsPbI₃ even though they may contain residual amounts of the parent anion.

Figure 3 compares the change in fluorescence intensity integrated over the entire microscope field-of-view during anion exchange to representative trajectories for individual NCs. For flow rates between 10 and 25 mL/h used to introduce the TBAI or TBAB solution, the transformation times were independent of the flow rate (Figure S7), and a flow rate of 20 mL/h was used in the experiments described below. Furthermore, the transformation times of individual NCs were independent of their position within the field-of-view (Figure S8), indicating that the reaction trajectories are controlled by the solid-state transformation of each NC rather than the diffusion of anions in solution. The ensemble trajectories shown in the top panels of Figure 3 include hundreds of single-particle trajectories (only portions of the field-of-view are shown in Figure 2b-e). As shown in the bottom panels of Figure 3, individual NCs undergo relatively sharp transitions relative to the ensemble. A comparison of ensemble rise times at different concentrations of substitutional ions to the mean intensity rise for individual NCs undergoing anion exchange is provided in Figure S9. The PL intensities of individual NCs start to rise at different times (marked by the dashed lines in Figure 3). Thus, the ensemble intensity rise incorporates the intensity rises of individual NCs as well as different waiting times before each NC starts to react. Notably, the trajectories of CsPbI₃ NCs transforming to CsPbBr₃ exhibit sharper rises in intensity compared to the trajectories of CsPbBr₃ NCs transforming to CsPbI₃ at both the ensemble and single-particle levels.

We quantified differences in the trajectories of individual NCs based on both the waiting time for the emission intensity of each NC to start increasing and the switching time or steepness of the intensity rise. To minimize the number of clusters that were

The Journal of Physical Chemistry C

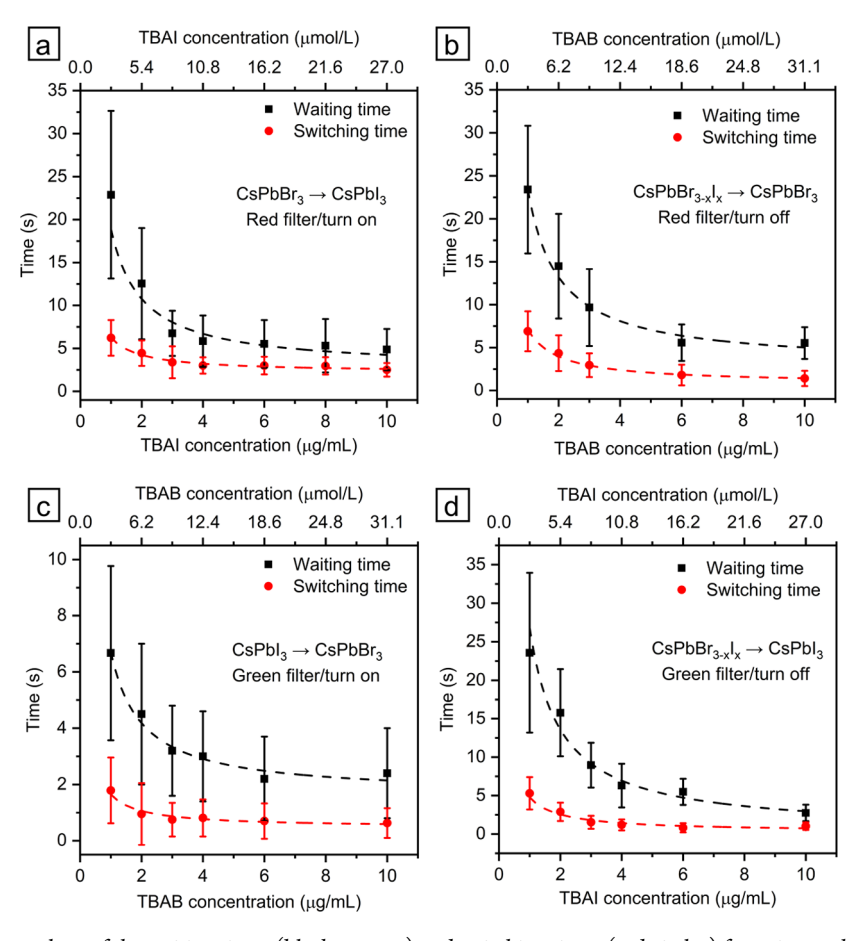


Figure 4. Experimental mean values of the waiting times (black squares) and switching times (red circles) for anion exchange between CsPbBr₃ and CsPbI₃ NCs. (a) Transformation of CsPbBr₃ NCs to CsPbI₃. (b) Back conversion of iodide-rich CsPbBr₃. $_{x}I_{x}$ NCs (prepared by anion exchange of CsPbBr₃ prior to imaging) to CsPbBr₃. (c) Transformation of CsPbI₃ NCs to CsPbBr₃. (d) Back conversion of bromide-rich CsPbBr₃. $_{x}I_{x}$ NCs (prepared by anion exchange of CsPbI₃ prior to imaging) to CsPbI₃. The error bars for each data point indicate the standard deviation of the waiting/ switching times. The dashed lines in each plot are fits to the concentration dependence of the form y = a/x + b. The fitted values of a and b are summarized in Table S4.

included in this analysis, we only analyzed trajectories that exhibited fluorescence intermittency with clear "on" and "off" states that are typically observed in the intensity trajectories of single particles (see Figure S10 for examples).¹³ Intensity trajectories with multiple on states and without a clear off state indicate a cluster of particles (i.e., multiple particles emitting within a diffraction-limited spot size, see Figure S11 for examples) and were excluded from subsequent analysis. The waiting time was measured as the time it took for the intensity of the NC to reach a value of 5σ over the mean background intensity before the reaction (where σ is the standard deviation in background intensity). Because it is difficult to measure the exact time the TBAI or TBAB solution enters the field-of-view under the microscope, the first NC to transform was given a waiting time of 0 s, and the waiting times of subsequent transformations were measured relative to the first one. Histograms of the distributions of waiting times for the conversion of CsPbBr₃ NCs to CsPbBrI₃, CsPbI₃ NCs to CsPbBr₃, and CsPbBr_{3-x}I₃ NCs (produced by anion exchange prior to imaging) to both CsPbBr3 and CsPbI3 are shown in Figures S12-S15. We fitted each distribution to a Gaussian function to extract both the mean value and the standard deviation of waiting times (Figure S16). The switching time for each NC was measured based on a sigmoidal fit of its intensity rise; a steeper rise in intensity gives a smaller value for the

switching time. Similar to the waiting times, for each transformation we extracted the mean switching time and standard deviation from Gaussian fitting of the distribution of switching times.

To understand the asymmetric behavior observed in ensemble PL spectra at different concentrations of the substitutional anion, we performed each transformation over a range of TBAI/TBAB concentrations (i.e., 1, 2, 3, 4, 6, 10 μ g/ mL) and measured the resulting distributions of waiting and switching times. For the transformation of CsPbBr₃ NCs to CsPbI₃, shown in Figure 4a, the mean and standard deviation of waiting times decreased from 22.8 \pm 9.7 to 4.8 \pm 2.4 s as the concentration of TBAI increased from 1 to 10 μ g/mL (2.7 to 27.0 μ mol/L). The mean and standard deviation of switching times for this transformation decreased from 6.2 ± 2.1 to $2.5 \pm$ 0.8 s as the concentration of TBAI increased from 1 to 10 μ g/ mL. The concentration dependencies of the waiting and switching times for the transformation of CsPbI₃ NCs to CsPbBr3 are shown in Figure 4c. The mean waiting and switching times and their standard deviations decreased from 6.7 \pm 3.1 to 2.4 \pm 1.6 s and from 1.8 \pm 1.2 to 0.6 \pm 0.5 s, respectively, as the concentration of TBAB increased from 1 to 10 μ g/mL (3.1 to 31.1 μ mol/L). Thus, in both exchange directions the waiting and switching times decreased as the concentration of TBAB/TBAI increased. The shorter waiting and switching times

The Journal of Physical Chemistry C

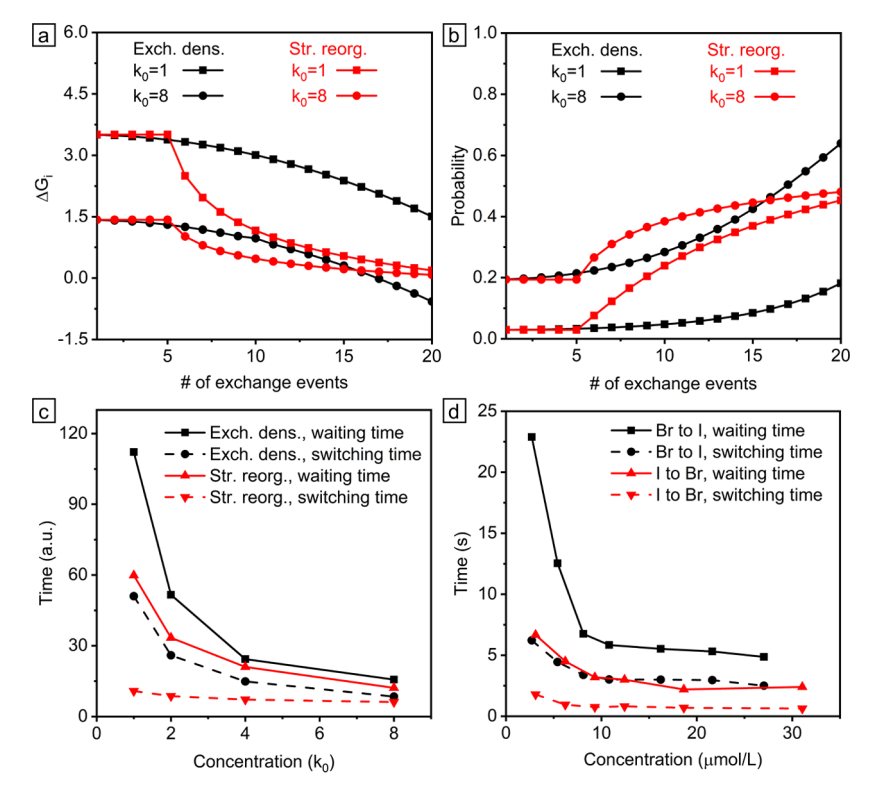


Figure 5. (a) Change in free energy, ΔG_p with the number of exchange events, *i*, in a particle for the exchange-density (Exch. dens., black traces) and structural-reorganization (Str. reorg., red traces) models. In each model, the initial free energy, ΔG_1 , was varied to simulate the effect of concentration. Plots for the minimum (i.e., $k_0 = 1$, squares) and maximum (i.e., $k_0 = 8$, circles) concentrations simulated are shown. (b) Associated probability of exchange for the models shown in (a). (c) Simulated waiting and switching times for the two models as a function of k_0 . (d) Experimental waiting and switching times for the conversion of as-synthesized CsPbI₃ NCs to CsPbBr₃ (red traces) and the back conversion of bromide-rich CsPbBr_{3-x}I_x NCs to CsPbI₃ (black traces).

for the transformation of CsPbI₃ NCs to CsPbBr₃ at low TBAB concentrations (along with the narrower distribution of waiting times) lead to the sharper rise in intensity for the ensemble of particles shown in Figure 3b.

The mean values of the waiting and switching times for anion exchange and their dependence on concentration showed significant differences in the two exchange directions. The mean waiting time for the conversion of CsPbBr₃ NCs to CsPbI₃ was 16 s longer than the conversion of CsPbI₃ NCs to CsPbBr₃ when using 1 μ g/mL of TBAI or TBAB. The difference between mean waiting times decreased at higher concentrations of the substitutional anion with only a 2-s difference at 10 μ g/mL. The mean waiting times for the conversion of CsPbBr₃ NCs to CsPbI₃ decreased by 80% as the concentration increased from 1 to 10 μ g/mL, while they only decreased by 60% for the conversion of CsPbI₃ NCs to CsPbBr₃. The mean switching times also showed differences in their concentration dependence in each exchange direction. The mean switching times for the conversion of CsPbBr₃ NCs to CsPbI₃ decreased by 50% as the TBAI concentration increased from 2 to 10 μ g/mL, while the mean switching times for the conversion of CsPbI₃ NCs to CsPbBr₃ decreased by only 30% over the same concentration range of TBAB. Overall, the mean waiting and switching times for the conversion of as-synthesized CsPbBr₃ NCs to CsPbI₃ exhibited a stronger dependence on the concentration of the substitutional ion.

Mixed-halide $CsPbBr_{3-x}I_x$ nanocrystals produced by anion exchange exhibited similar mean waiting and switching times to those of the as-synthesized $CsPbBr_3$ NCs undergoing exchange to $CsPbI_3$ regardless of the exchange direction. We converted

CsPbBr₃ NCs to iodide-rich CsPbBr_{3-x}I_x and then imaged their back conversion under the microscope to CsPbBr₃ using different concentrations of TBAB (Figure 4b). Using the red filter set, we observed that the initially bright fluorescent spots in the field-of-view become dark as the transformation progressed. The mean waiting and switching times and their standard deviations decreased from 23.4 \pm 7.4 to 5.5 \pm 1.8 s and from 6.9 \pm 2.3 to 1.4 \pm 0.9 s, respectively, as the concentration of TBAB increased from 1 to 10 μ g/mL (3.1 to 31.1 μ mol/L). These values for back exchange are significantly longer than the transformation of as-synthesized CsPbI3 NCs to CsPbBr3 and closely match those of the CsPbBr₃ to CsPbI₃ reaction. We also converted CsPbI₃ NCs to bromide-rich CsPbBr_{3-x}I_x and then imaged their back conversion to CsPbI3 under the microscope using the green filter set to watch the turn off in emission (Figure 4d). Similar to the iodide-rich CsPbBr_{3-x}I_x NCs undergoing back conversion, the mean waiting and switching times and their standard deviation decreased from 23.6 \pm 10.4 to 2.7 \pm 1.1 s and from 5.3 ± 2.1 to 1.0 ± 0.5 s, respectively, as the concentration of TBAI increased from 1 to 10 μ g/mL (2.7 to 27.0 μ mol/L).

Monte Carlo Model for Asymmetric Anion Exchange. We reasoned that the asymmetric behavior observed in both ensemble and single-particle fluorescence studies arises from differences in the reaction path during anion exchange in opposite directions. To support this hypothesis, we used Monte Carlo trajectories to simulate anion exchange in individual particles and their waiting and switching times (see the SI for details of the simulations). In these simulations, differences in the reaction path are reflected in the way the probability for each exchange event in a particle evolves with the number of previous

successful events. The incorporation of positive cooperativity where previous events make future ones more probable produces sharp transitions for individual particles to transform along with a distribution of waiting times. ^{39–42} We find that the degree of cooperativity or how much the probability changes with each previous event controls the sharpness of transitions (i.e., the switching times) as well as the concentration dependence of waiting and switching times.

The waiting and switching times for the transformation of assynthesized CsPbBr3 NCs to CsPbI3 (as well as the back conversion of mixed-halide CsPbBr_{3-x}I_x NCs) closely resemble our previous work on anion exchange between CsPbCl3 and CsPbBr₃ NCs.⁴² In this previous study, we showed that the concentration dependence of waiting and switching times for highly miscible systems can be reproduced when the probability gradually increases with the number of successive exchange events. The black traces in Figure 5a,b show the simulated changes in free energy and the associated probability of exchange events for this exchange-density model in which the change in free energy for anion exchange in a particle is proportional to the density of exchanged ions. The concave downward curvature for the change in free energy leads to a gradual increase in the probability with successive exchange events. Changes in the concentration of substitutional anions were simulated by varying the initial probability (see the SI for details). We varied the simulated concentration over a similar range to the experimental variations in concentration (in $\mu g/mL$ of TBAI/TBAB) shown in Figure 4. The simulated concentration dependencies of waiting and switching times for the exchange-density model and corresponding experimental times for the back conversion of bromide-rich CsPbBr_{3-x}I_x NCs to CsPbI₃ are shown in Figure 5c,d (black traces). We use this sample for comparison as it will have nearly the same size distribution as the as-synthesized CsPbI₃ NCs that were used to prepare it. Based on the similarities in experimental waiting and switching times shown in Figure 4, this model also applies to the conversion of as-synthesized CsPbBr3 NCs to CsPbI3 and the back conversion of iodide-rich CsPbBr_{3-x}I_x NCs to CsPbBr₃. The exchange-density model reproduces the longer waiting and switching times for these samples (see Figure S17) as well as their steeper dependence on concentration (at low concentrations of substitutional anions) relative to the conversion of CsPbI₃ NCs to CsPbBr₃ described below. Furthermore, both the exchange-density model and the experimental values for the back conversion of bromide-rich CsPbBr_{3-x}I_x NCs to CsPbI₃ show a linear correlation between the waiting and switching times of individual particles. As shown in Figure S18a,b, particles with longer waiting times are more likely to have longer switching times. Linear fits to the distribution of waiting and switching times for individual particles give average slopes of 0.15 ± 0.01 (average \pm 1st standard deviation for different concentrations) for the exchange-density model and 0.11 ± 0.03 for the experimental results (see Figure S19 and Table S5 for details). This correlation occurs because the slower rises in intensity for individual particles (especially at lower concentrations of TBAI) lead to an overlap between the measurements of waiting and switching times.

Previous work from our group and that of Routzahn and Jain have shown that the waiting and switching times for the transformation of immiscible crystal pairs (e.g., CdSe/Ag₂Se and PbBr₂/CH₃NH₃PbBr₃) that require a substantial reorganization in structure can be reproduced by incorporating an abrupt increase in the probability during the Monte Carlo trajecto-

ries.^{39–41} For example, in our previous model used to describe the intercalation of CH₃NH₃Br into PbBr₂ NCs in which a new phase must nucleate in each particle, the initial reaction events have equal probability. However, after a critical number of events have taken place in a particle, the free-energy change associated with each successive event abruptly decreases and the associated probability increases. The conversion of assynthesized CsPbI₃ NCs to CsPbBr₃ studied here appears to be an intermediate case between the fully miscible and fully immiscible systems that have been previously modeled. While the transformation of CsPbI₃ NCs does not require a distinct phase change, it likely involves a coordinated reorganization of the tilt angles of corner-sharing PbX₆ octahedra (discussed in more detail below). Thus, we adapted our previous model to the conversion of CsPbI₃ NCs to CsPbBr₃ by adjusting the curvature in free energy after the threshold such that the change in the probability was less abrupt (see the SI for further details). The red traces in Figure 5a,b show the simulated changes in free energy and probability for exchange events using this structuralreorganization model. The initial events have equal probability, but after a critical threshold (five in these simulations), the freeenergy change associated with each successive event decreases and the probability increases. The concave upward curvature for the change in free energy with reaction events after the threshold (and concave downward curvature of the probability) leads to a change in the probability that successfully models the sharper switching times for this transformation (Figure S17). The simulated concentration dependencies of waiting and switching times for the structural-reorganization model and corresponding experimental times for the conversion of CsPbI₃ NCs to CsPbBr₃ are shown in Figure 5c,d (red traces). The structuralreorganization model reproduces both the shorter waiting and switching times seen experimentally for this transformation and their relative insensitivity to concentration. The larger structural reorganization needed during the conversion of CsPbI₃ NCs to CsPbBr₃ also leads to a greater temporal separation between the waiting and switching times. In both the Monte Carlo simulations using the structural-reorganization model and the experimental values for the conversion of CsPbI₃ NCs to CsPbBr₃, there is no correlation between these values at low concentrations (Figure S18c,d). However, at the highest simulated concentration, the changes in free energy and probability for exchange events in the two models are similar (see the traces marked with circles in Figure 5a,b). Consequently, the respective waiting and switching times for the two models also have more similar mean values at the highest simulated concentration (Figure 5c) in agreement with the experimental results (Figure 5d).

Our single-particle fluorescence studies supported by Monte Carlo simulations reveal that $CsPbI_3$ nanocrystals synthesized by the hot-injection method undergo an abrupt structural reorganization as they transform to $CsPbBr_3$. We postulate that this structural reorganization involves coordinated changes in the titling patterns of PbX_6 octahedra. The in-plane and out-of-plane tilt angles of PbX_6 octahedra are different in bulk $CsPbBr_3$ and $CsPbI_3$ with the perovskite orthorhombic γ structure due to the different radii of Br^- (1.82 Å) and I^- (2.06 Å) anions (see Table S6). $CsPbBr_3$ and $CsPbI_3$ NCs also show differences in their octahedral tilting patterns. ^{12,27,48} Furthermore, Zhao and co-workers recently reported size-dependent structural variations in size-selected $CsPbI_3$ NCs with the orthorhombic γ phase for edge lengths up to 15.3 nm that arise from surface strain. ²⁹ Rietveld refinement of powder XRD

patterns indicated there were variations in the octahedral tilt angles as a function of NC size. While the size distributions of our CsPbX $_3$ samples are too broad to perform Rietveld refinement and measure changes in the octahedral tilt angles, the mean size of our initial CsPbI $_3$ NCs (11.9 nm) falls within the range where surface strain is expected to induce changes to their structure. Thus, the octahedral tilt angles likely change during anion exchange both due to differences in bulk structure along with the different surface energies associated with CsPbBr $_3$ and CsPbI $_3$.

A more abrupt structural reorganization during the conversion of the as-synthesized CsPbI3 NCs to CsPbBr3 is consistent with the narrower distributions of waiting and switching times observed for this transformation (see Figures S16 and S18). This structural reorganization also explains the peak splitting observed in ensemble PL spectra during the conversion of CsPbI₃ NCs to CsPbBr₃. The interconversion between the two distinct populations of iodide-rich and bromide-rich CsPbBr_{3-r}I_r NCs likely coincides with the reordering of the PbX₆ octahedra. On the other hand, CsPbBr₃ NCs undergo a smooth transition to CsPbI₃, indicating that the tilting pattern of the initial CsPbBr3 NCs is largely conserved during their transformation. This smooth transition leads to longer waiting and switching times with a wider distribution at low concentrations of substitutional anions. Furthermore, CsPbBr_{3-x}I_x nanocrystals that have already undergone anion exchange possess similar mean waiting and switching times to those of the as-synthesized CsPbBr₃ NCs undergoing exchange to CsPbI₃. This indicates that when bromide-rich CsPbBr_{3-x}I_x NCs produced by anion exchange of CsPbI₃ are converted back to CsPbI₃ they retain a structure similar to the CsPbBr₃ NCs. Thus, we propose that anion exchange between as-synthesized CsPbBr₃ and CsPbI₃ NCs is not reversible and that CsPbI₃ NCs produced by anion exchange do not have the same structure as those produced by hot injection.

CONCLUSIONS

In summary, we used single-particle fluorescence to elucidate asymmetric chemical reactivity during anion exchange between CsPbBr₃ and CsPbI₃ nanocrystals. We attribute shorter reaction times for individual CsPbI₃ NCs along with a narrower distribution to a more abrupt structural reorganization needed as they transform to CsPbBr₃. CsPbBr₃ NCs do not undergo this structural reorganization as they transform to CsPbI₃, leading to a wider distribution of reaction times. Our study indicates that subtle structural differences between CsPbX3 nanocrystals that are difficult to detect by conventional powder X-ray diffraction can have a significant impact on their chemical reactivity. X-ray total scattering measurements using synchrotron radiation could be used in the future to quantify differences in the structure of CsPbI₃ NCs made by the hot-injection method vs by anion exchange. 27,28,52 While our studies were performed under dilute conditions (i.e., isolated nanocrystals dispersed on a substrate), the distribution of reaction times may affect the compositional homogeneity of CsPbX₃ NCs produced by anion exchange at higher concentrations, which will be needed to scale-up this reaction. If the local concentration of substitutional anions becomes depleted, then NCs with longer waiting times will incorporate a lower fraction of the substitutional anion. This inherent distribution of reaction times, which is controlled by the degree of structural reorganization during the nanocrystal transformation, is important to consider when developing scaled-up fabrication routes that maximize the color purity of luminescent CsPbX₃ nanocrystals for optoelectronic devices.

ASSOCIATED CONTENT

5 Supporting Information

The Supporting Information is available free of charge at https://pubs.acs.org/doi/10.1021/acs.jpcc.0c08323.

Experimental details on additional structural characterization by XRD and TEM, the fabrication of flow cells for fluorescence microscopy, analysis of fluorescence videos, and Monte Carlo simulations; supporting tables providing the peak positions of fluorescence spectra and their FWHM, a list of the samples characterized in different figures, fitting parameters for the concentration dependence of waiting and switching times, fitting parameters for plots of waiting vs switching times, and the octahedral tilt angles of bulk CsPbBr3 and CsPbI3; supporting figures showing additional PL spectra of CsPbX₃ NCs before and after anion exchange, structural characterization by TEM and XRD, waiting times as a function of flow rate, particle position, and TBAB or TBAI concentration, a comparison of the mean of individual NC switching times to the ensemble intensity rise, a comparison of fluorescence intensity trajectories for single NCs and clusters of particles, simulated reaction trajectories for different Monte Carlo simulations, and plots of the waiting time vs switching time for individual NCs (PDF)

Fluorescence video using the red filter set in which individual nanocrystals become bright as they transform from $CsPbBr_3$ to $CsPbI_3$ (Movie M1) (MP4)

Fluorescence video using the red filter set in which individual nanocrystals become dark as they undergo back conversion from $CsPbBr_{3-x}I_x$ to $CsPbBr_3$ (Movie M2) (MP4)

Fluorescence video using the green filter set in which individual nanocrystals become bright as they transform from CsPbI₃ to CsPbBr₃ (Movie M3) (MP4)

Fluorescence video using the green filter set in which individual nanocrystals become dark as they undergo back conversion from $CsPbBr_{3-x}I_x$ to $CsPbI_3$ (Movie M4) (MP4)

AUTHOR INFORMATION

Corresponding Author

Bryce Sadtler — Department of Chemistry and Institute of Materials Science & Engineering, Washington University, St. Louis, Missouri 63130, United States; orcid.org/0000-0003-4860-501X; Email: sadtler@wustl.edu

Authors

Dong Wang — Department of Chemistry, Washington University, St. Louis, Missouri 63130, United States; orcid.org/0000-0002-7268-3483

Dongyan Zhang – Department of Chemistry, Washington University, St. Louis, Missouri 63130, United States

Complete contact information is available at: https://pubs.acs.org/10.1021/acs.jpcc.0c08323

Notes

I

The authors declare no competing financial interest.

ACKNOWLEDGMENTS

This material is based upon work supported by the National Science Foundation (NSF) under grant no. CHE-1753344. Acknowledgment is made to the donors of the American Chemical Society Petroleum Research Fund for partial support of this research (award # PRF58165-DNI10). Electron microscopy was performed at the Institute of Materials Science & Engineering at Washington University. X-ray diffraction was performed in the Department of Earth and Planetary Sciences at Washington University. The Authors thank J. Cavin, R. Mishra, and L. Sobotka for useful discussions.

REFERENCES

- (1) Green, M. A.; Ho-Baillie, A.; Snaith, H. J. The Emergence of Perovskite Solar Cells. *Nat. Photonics* **2014**, *8*, 506–514.
- (2) Lin, Q.; Armin, A.; Nagiri, R. C. R.; Burn, P. L.; Meredith, P. Electro-Optics of Perovskite Solar Cells. *Nat. Photonics* **2014**, *9*, 106–112.
- (3) Wang, D.; Liu, Z.; Zhou, Z.; Zhu, H.; Zhou, Y.; Huang, C.; Wang, Z.; Xu, H.; Jin, Y.; Fan, B.; et al. Reproducible One-Step Fabrication of Compact MAPbI_{3-x}Cl_x Thin Films Derived from Mixed-Lead-Halide Precursors. *Chem. Mater.* **2014**, *26*, 7145–7150.
- (4) Xiao, Z.; Kerner, R. A.; Zhao, L.; Tran, N. L.; Lee, K. M.; Koh, T.-W.; Scholes, G. D.; Rand, B. P. Efficient Perovskite Light-Emitting Diodes Featuring Nanometre-Sized Crystallites. *Nat. Photonics* **2017**, *11*, 108–115.
- (5) Wang, N.; Cheng, L.; Ge, R.; Zhang, S.; Miao, Y.; Zou, W.; Yi, C.; Sun, Y.; Cao, Y.; Yang, R.; et al. Perovskite Light-Emitting Diodes Based on Solution-Processed Self-Organized Multiple Quantum Wells. *Nat. Photonics* **2016**, *10*, 699–704.
- (6) Rainò, G.; Becker, M. A.; Bodnarchuk, M. I.; Mahrt, R. F.; Kovalenko, M. V.; Stöferle, T. Superfluorescence from Lead Halide Perovskite Quantum Dot Superlattices. *Nature* **2018**, *563*, *671*–*675*.
- (7) Utzat, H.; Sun, W.; Kaplan, A. E. K.; Krieg, F.; Ginterseder, M.; Spokoyny, B.; Klein, N. D.; Shulenberger, K. E.; Perkinson, C. F.; Kovalenko, M. V.; et al. Coherent Single-Photon Emission from Colloidal Lead Halide Perovskite Quantum Dots. *Science* **2019**, *363*, 1068–1072.
- (8) Protesescu, L.; Yakunin, S.; Bodnarchuk, M. I.; Krieg, F.; Caputo, R.; Hendon, C. H.; Yang, R. X.; Walsh, A.; Kovalenko, M. V. Nanocrystals of Cesium Lead Halide Perovskites (CsPbX₃, X = Cl, Br, and I): Novel Optoelectronic Materials Showing Bright Emission with Wide Color Gamut. *Nano Lett.* **2015**, *15*, 3692–3696.
- (9) Swarnkar, A.; Chulliyil, R.; Ravi, V. K.; Irfanullah, M.; Chowdhury, A.; Nag, A. Colloidal CsPbBr₃ Perovskite Nanocrystals: Luminescence Beyond Traditional Quantum Dots. *Angew. Chem., Int. Ed.* **2015**, *54*, 15424–15428.
- (10) Bekenstein, Y.; Koscher, B. A.; Eaton, S. W.; Yang, P.; Alivisatos, A. P. Highly Luminescent Colloidal Nanoplates of Perovskite Cesium Lead Halide and Their Oriented Assemblies. *J. Am. Chem. Soc.* **2015**, 137, 16008–16011.
- (11) Di Stasio, F.; Christodoulou, S.; Huo, N.; Konstantatos, G. Near-Unity Photoluminescence Quantum Yield in CsPbBr₃ Nanocrystal Solid-State Films Via Postsynthesis Treatment with Lead Bromide. *Chem. Mater.* **2017**, *29*, 7663–7667.
- (12) Creutz, S. E.; Crites, E. N.; De Siena, M. C.; Gamelin, D. R. Anion Exchange in Cesium Lead Halide Perovskite Nanocrystals and Thin Films Using Trimethylsilyl Halide Reagents. *Chem. Mater.* **2018**, *30*, 4887–4891.
- (13) Zhang, A.; Dong, C.; Ren, J. Tuning Blinking Behavior of Highly Luminescent Cesium Lead Halide Nanocrystals through Varying Halide Composition. *J. Phys. Chem. C* **2017**, *121*, 13314–13323.
- (14) Yoshimura, H.; Yamauchi, M.; Masuo, S. In Situ Observation of Emission Behavior During Anion-Exchange Reaction of a Cesium Lead Halide Perovskite Nanocrystal at the Single-Nanocrystal Level. *J. Phys. Chem. Lett.* **2020**, *11*, 530–535.

- (15) Nedelcu, G.; Protesescu, L.; Yakunin, S.; Bodnarchuk, M. I.; Grotevent, M. J.; Kovalenko, M. V. Fast Anion-Exchange in Highly Luminescent Nanocrystals of Cesium Lead Halide Perovskites (CsPbX₃, X = Cl, Br, I). *Nano Lett.* **2015**, *15*, 5635–5640.
- (16) Akkerman, Q. A.; D'Innocenzo, V.; Accornero, S.; Scarpellini, A.; Petrozza, A.; Prato, M.; Manna, L. Tuning the Optical Properties of Cesium Lead Halide Perovskite Nanocrystals by Anion Exchange Reactions. *J. Am. Chem. Soc.* **2015**, *137*, 10276–10281.
- (17) Hoffman, J. B.; Schleper, A. L.; Kamat, P. V. Transformation of Sintered CsPbBr₃ Nanocrystals to Cubic CsPbI₃ and Gradient CsPbBr_xI_{3-x} through Halide Exchange. *J. Am. Chem. Soc.* **2016**, *138*, 8603–8611.
- (18) Pellet, N.; Teuscher, J.; Maier, J.; Grätzel, M. Transforming Hybrid Organic Inorganic Perovskites by Rapid Halide Exchange. *Chem. Mater.* **2015**, *27*, 2181–2188.
- (19) Koscher, B. A.; Bronstein, N. D.; Olshansky, J. H.; Bekenstein, Y.; Alivisatos, A. P. Surface- vs Diffusion-Limited Mechanisms of Anion Exchange in CsPbBr₃ Nanocrystal Cubes Revealed through Kinetic Studies. *J. Am. Chem. Soc.* **2016**, *138*, 12065–12068.
- (20) Li, M.; Zhang, X.; Lu, S.; Yang, P. Phase Transformation, Morphology Control, and Luminescence Evolution of Cesium Lead Halide Nanocrystals in the Anion Exchange Process. *RSC Adv.* **2016**, *6*, 103382–103389.
- (21) Rosales, B. A.; Men, L.; Cady, S. D.; Hanrahan, M. P.; Rossini, A. J.; Vela, J. Persistent Dopants and Phase Segregation in Organolead Mixed-Halide Perovskites. *Chem. Mater.* **2016**, *28*, 6848–6859.
- (22) Bertolotti, F.; Protesescu, L.; Kovalenko, M. V.; Yakunin, S.; Cervellino, A.; Billinge, S. J. L.; Terban, M. W.; Pedersen, J. S.; Masciocchi, N.; Guagliardi, A. Coherent Nanotwins and Dynamic Disorder in Cesium Lead Halide Perovskite Nanocrystals. *ACS Nano* **2017**, *11*, 3819–3831.
- (23) Pan, D.; Fu, Y.; Chen, J.; Czech, K. J.; Wright, J. C.; Jin, S. Visualization and Studies of Ion-Diffusion Kinetics in Cesium Lead Bromide Perovskite Nanowires. *Nano Lett.* **2018**, *18*, 1807–1813.
- (24) Haque, A.; Ravi, V. K.; Shanker, G. S.; Sarkar, I.; Nag, A.; Santra, P. K. Internal Heterostructure of Anion-Exchanged Cesium Lead Halide Nanocubes. *J. Phys. Chem. C* **2018**, *122*, 13399–13406.
- (25) Yin, W.-J.; Yan, Y.; Wei, S.-H. Anomalous Alloy Properties in Mixed Halide Perovskites. J. Phys. Chem. Lett. 2014, 5, 3625–3631.
- (26) Bechtel, J. S.; Van der Ven, A. First-Principles Thermodynamics Study of Phase Stability in Inorganic Halide Perovskite Solid Solutions. *Phys. Rev. Mater.* **2018**, *2*, No. 045401.
- (27) Cottingham, P.; Brutchey, R. L. On the Crystal Structure of Colloidally Prepared CsPbBr₃ Quantum Dots. *Chem. Commun.* **2016**, 52, 5246–5249.
- (28) Cottingham, P.; Brutchey, R. L. Compositionally Dependent Phase Identity of Colloidal CsPbBr $_{3-x}I_x$ Quantum Dots. *Chem. Mater.* **2016**, 28, 7574–7577.
- (29) Zhao, Q.; Hazarika, A.; Schelhas, L. T.; Liu, J.; Gaulding, E. A.; Li, G.; Zhang, M.; Toney, M. F.; Sercel, P. C.; Luther, J. M. Size-Dependent Lattice Structure and Confinement Properties in CsPbI₃ Perovskite Nanocrystals: Negative Surface Energy for Stabilization. *ACS Energy Lett.* **2020**, *5*, 238–247.
- (30) Empedocles, S.; Bawendi, M. Spectroscopy of Single CdSe Nanocrystallites. *Acc. Chem. Res.* **1999**, *32*, 389–396.
- (31) Zhu, F.; Men, L.; Guo, Y.; Zhu, Q.; Bhattacharjee, U.; Goodwin, P. M.; Petrich, J. W.; Smith, E. A.; Vela, J. Shape Evolution and Single Particle Luminescence of Organometal Halide Perovskite Nanocrystals. *ACS Nano* **2015**, *9*, 2948–2959.
- (32) Park, Y.-S.; Guo, S.; Makarov, N. S.; Klimov, V. I. Room Temperature Single-Photon Emission from Individual Perovskite Quantum Dots. *ACS Nano* **2015**, *9*, 10386–10393.
- (33) Rainò, G.; Nedelcu, G.; Protesescu, L.; Bodnarchuk, M. I.; Kovalenko, M. V.; Mahrt, R. F.; Stöferle, T. Single Cesium Lead Halide Perovskite Nanocrystals at Low Temperature: Fast Single-Photon Emission, Reduced Blinking, and Exciton Fine Structure. *ACS Nano* **2016**, *10*, 2485–2490.
- (34) Utzat, H.; Shulenberger, K. E.; Achorn, O. B.; Nasilowski, M.; Sinclair, T. S.; Bawendi, M. G. Probing Linewidths and Biexciton

- Quantum Yields of Single Cesium Lead Halide Nanocrystals in Solution. *Nano Lett.* **2017**, *17*, 6838–6846.
- (35) Freppon, D. J.; Men, L.; Burkhow, S. J.; Petrich, J. W.; Vela, J.; Smith, E. A. Photophysical Properties of Wavelength-Tunable Methylammonium Lead Halide Perovskite Nanocrystals. *J. Mater. Chem. C* 2017, 5, 118–126.
- (36) Gibson, N. A.; Koscher, B. A.; Alivisatos, A. P.; Leone, S. R. Excitation Intensity Dependence of Photoluminescence Blinking in CsPbBr₃ Perovskite Nanocrystals. *J. Phys. Chem. C* **2018**, *122*, 12106–12113.
- (37) Seth, S.; Ahmed, T.; Samanta, A. Photoluminescence Flickering and Blinking of Single CsPbBr₃ Perovskite Nanocrystals: Revealing Explicit Carrier Recombination Dynamics. *J. Phys. Chem. Lett.* **2018**, *9*, 7007–7014.
- (38) Yuan, G.; Ritchie, C.; Ritter, M.; Murphy, S.; Gómez, D. E.; Mulvaney, P. The Degradation and Blinking of Single CsPbI₃ Perovskite Quantum Dots. *J. Phys. Chem. C* **2018**, *122*, 13407–13415.
- (39) Routzahn, A. L.; Jain, P. K. Single-Nanocrystal Reaction Trajectories Reveal Sharp Cooperative Transitions. *Nano Lett.* **2014**, 14, 987–992.
- (40) Routzahn, A. L.; Jain, P. K. Luminescence Blinking of a Reacting Quantum Dot. *Nano Lett.* **2015**, *15*, 2504–2509.
- (41) Yin, B.; Cavin, J.; Wang, D.; Khan, D.; Shen, M.; Laing, C.; Mishra, R.; Sadtler, B. Fluorescence Microscopy of Single Lead Bromide Nanocrystals Reveals Sharp Transitions During Their Transformation to Methylammonium Lead Bromide. *J. Mater. Chem. C* **2019**, *7*, 3486–3495.
- (42) Wang, D.; Cavin, J.; Yin, B.; Thind, A. S.; Borisevich, A. Y.; Mishra, R.; Sadtler, B. Role of Solid-State Miscibility During Anion Exchange in Cesium Lead Halide Nanocrystals Probed by Single-Particle Fluorescence. *J. Phys. Chem. Lett.* **2020**, *11*, 952–959.
- (43) Karimata, I.; Tachikawa, T. In Situ Exploration of the Structural Transition During Morphology- and Efficiency-Conserving Halide Exchange on a Single Perovskite Nanocrystal. *Angew. Chem., Int. Ed.* **2020**, No. 202013386.
- (44) Smith, A. M.; Nie, S. Bright and Compact Alloyed Quantum Dots with Broadly Tunable Near-Infrared Absorption and Fluorescence Spectra through Mercury Cation Exchange. *J. Am. Chem. Soc.* **2011**, 133, 24–26.
- (45) White, S. L.; Smith, J. G.; Behl, M.; Jain, P. K. Co-Operativity in a Nanocrystalline Solid-State Transition. *Nat. Commun.* **2013**, 4, No. 2933.
- (46) Orfield, N. J.; McBride, J. R.; Keene, J. D.; Davis, L. M.; Rosenthal, S. J. Correlation of Atomic Structure and Photoluminescence of the Same Quantum Dot: Pinpointing Surface and Internal Defects That Inhibit Photoluminescence. *ACS Nano* **2015**, *9*, 831–839.
- (47) Ryan, D. P.; Goodwin, P. M.; Sheehan, C. J.; Whitcomb, K. J.; Gelfand, M. P.; Van Orden, A. Mapping Emission from Clusters of CdSe/ZnS Nanoparticles. *J. Phys. Chem. C* **2018**, *122*, 4046–4053.
- (48) Marronnier, A.; Roma, G.; Boyer-Richard, S.; Pedesseau, L.; Jancu, J.-M.; Bonnassieux, Y.; Katan, C.; Stoumpos, C. C.; Kanatzidis, M. G.; Even, J. Anharmonicity and Disorder in the Black Phases of Cesium Lead Iodide Used for Stable Inorganic Perovskite Solar Cells. *ACS Nano* **2018**, *12*, 3477–3486.
- (49) Yang, F.; Wang, C.; Pan, Y.; Zhou, X.; Kong, X.; Ji, W. Surface Stabilized Cubic Phase of CsPbI₃ and CsPbBr₃ at Room Temperature. *Chin. Phys. B* **2019**, *28*, 56402–056402.
- (50) Yang, R. X.; Tan, L. Z. Understanding Size Dependence of Phase Stability and Band Gap in CsPbI₃ Perovskite Nanocrystals. *J. Chem. Phys.* **2020**, *152*, No. 034702.
- (S1) Jeon, S.; Jung, M.-C.; Ahn, J.; Woo, H. K.; Bang, J.; Kim, D.; Lee, S. Y.; Woo, H. Y.; Jeon, J.; Han, M. J.; et al. Post-Synthetic Oriented Attachment of CsPbBr₃ Perovskite Nanocrystal Building Blocks: From First Principle Calculation to Experimental Demonstration of Size and Dimensionality (0D/1D/2D). *Nanoscale Horiz.* **2020**, *5*, 960–970.
- (52) Bertolotti, F.; Nedelcu, G.; Vivani, A.; Cervellino, A.; Masciocchi, N.; Guagliardi, A.; Kovalenko, M. V. Crystal Structure, Morphology, and Surface Termination of Cyan-Emissive, Six-Monolayers-Thick

CsPbBr₃ Nanoplatelets from X-Ray Total Scattering. ACS Nano 2019, 13, 14294–14307.